Forest Ecology and Management 567 (2024) 122071

Contents lists available at ScienceDirect

Forest Ecology and Management

journal homepage: www.elsevier.com/locate/foreco

Effect of repeated pulling loads on Norway spruce (*Picea abies* (L.) Karst.) trees

Luca Marchi [a,*], Maximiliano Costa [b], Barry Gardiner [c,d,e], Tommaso Locatelli [e], Emanuele Lingua [a]

[a] Department of Land, Environment, Agriculture and Forestry (TESAF), University of Padova, Legnaro, Padova, Italy
[b] Forest Ecology Professorship, Eidgenössische Technische Hochschule, Zürich, Switzerland
[c] Institut Européen De La Forêt Cultivée, Cestas, France
[d] Department of Forestry Economics and Forest Planning, Albert-Ludwigs-University Freiburg, Freiburg im Breisgau, Germany
[e] Forest Research, Northern Research Station, Roslin, Scotland, UK

ARTICLE INFO

Keywords:
Tree stability
Alpine ecosystem
Cyclic tests
Energy dissipation
Wind risk modelling

ABSTRACT

Artificial pulling tests are the most practical method of assessing the maximum resistance of trees to lateral forces (e.g., from the wind), particularly in relation to their anchoring capacity in the ground. The traditional method is to pull the tree monotonically until failure. However, there are still many uncertainties regarding the possibility of mimicking wind gusts in such a tree pulling test. More specifically, it is supposed that a succession of wind gusts during a windstorm may cause fatigue to the root system, leading to a propagation of damage at the root-soil interface which will eventually lead to the collapse of the tree. This work aims to provide initial insights into the biomechanical response of shallow-rooted Norway spruce (Picea abies (L.) Karst.) growing in mineral soils by repeatedly pulling to failure six trees with increasing load magnitude. The mechanical behaviour of the tested trees was first analysed using a classical equilibrium approach by calculating peak applied loads, stem base rotation, equivalent stiffness trend over subsequent cycles and residual rotations. Then, the biomechanics of the trees were analysed using an energetic approach, focusing on the energy absorbed and dissipated during either the single load cycle or the complete cyclic test, by applying consolidated procedures used in the field of mechanical engineering.

Results show how small but measurable residual rotations were measured after each load repetition, indicating permanent damage even in seemingly undamaged trees. Additionally, loads producing base rotations about 0.3–0.4 times those corresponding to the peak resistance dissipate less than 1 % of the maximum dissipated energy calculated at the same peak point. Additionally, this peak energy is found to be strongly correlated to both the peak moment and a typical stem volume predictor such as diameter at breast height squared times height.

All these outcomes are intended to provide a starting point for the development of a different characterisation of tree resistance as an alternative to the current methodologies, especially when it is important to consider the effects of repeated loading on trees.

1. Introduction

Understanding the mechanical response of living trees to environmental stressors is a challenging topic given the high quantity of variables that needs to be accounted for. Despite this, tree biomechanics has always been an area of great interest as it has the intrinsic potential to involve a large variety of end users and attracts the interest not only of people from the scientific community but also from practitioners and public authorities. Moreover, this knowledge can be useful not only for forest management (in the classical sense) but also for urban forestry. Attention to trees growing in the urban environment is increasing and the management of these plants is particularly important for public safety (Klein et al., 2019; Linhares et al., 2021).

Windstorms are responsible for severe damage to forest ecosystems in Europe (Laurance and Curran, 2008; Patacca et al., 2023; Romagnoli et al., 2023). Considering the mechanical response to natural disturbances, wind-tree interaction is one of the most extensively studied topics. The focus of these studies has been to explore the behaviour of trees at their limits, i.e., to analyse and predict their load bearing

* Corresponding author.
E-mail address: luca.marchi@unipd.it (L. Marchi).

https://doi.org/10.1016/j.foreco.2024.122071
Received 13 March 2024; Received in revised form 4 June 2024; Accepted 8 June 2024
Available online 26 June 2024

Abbreviations

E	is the energy evaluated from the M-θ relation
$E_{Dis,i}$	is the dissipated energy evaluated on the i^{th} load cycle
$E_{El,i}$	is the elastic energy evaluated on the i^{th} load cycle
$E_{Max,i}$	is the maximum input energy on the i^{th} load cycle
$E_{Max,c,i}$	is the maximum cumulative input energy at the i^{th} load cycle
$E_{Res,i}$	is the residual (unrecovered) energy after the i^{th} load cycle
$E_{Max,Peak}$	is the input energy evaluated at M_{Peak}
$K_{S,i}$	is the secant stiffness on the i^{th} load cycle
$K_{R,i}$	is the reloading stiffness on the i^{th} load cycle
M	applied moment
M_{Peak}	is the maximum applied moment in the test or overturning moment
$M_{Min,i}$; $M_{Max,i}$	are the minimum and maximum moments applied on the i^{th} load cycle
M_0	is the applied moment normalised by the overturning moment, i.e., M/M_{Peak}
θ	rotation of the root-plate system or stem base
$\theta(M_{Peak})$	is the rotation corresponding to M_{Peak}
$\theta(M_{Min,i})$; $\theta(M_{Max,i})$	are the rotations corresponding to $M_{Min,i}$ $M_{Max,I}$ obtained on the i^{th} load cycle
$\theta_{Max,i}$	is the maximum rotation registered at the end of the i^{th} load cycle
$\theta_{R,i}$	is the residual rotation registered at the end of the i^{th} load cycle
θ_0	is the rotation of the root plate (or stem base) normalised by the rotation corresponding to the overturning moment, i.e., $\theta/\theta(M_{Peak})$
Δθ	is the rotation increment at the peak load $M_{Max,i}$ between two consecutive cycles
χ	is the ratio K_S/K_R

capacity based on general allometric characteristics of both the specific tree as well as external factors such as the characteristics of the site (e.g., soil type, root depth (Coutts, 1986; Nicoll et al., 2006; Peltola et al., 2000)). The experimental setup of these studies shows that, currently, the only way to scientifically determine the ultimate resistance of a tree is via destructive tests, for which the most notable in-situ methodology is the tree pulling test. Thousands of pulling experiments have been performed and data collected to derive a robust database from which to start and develop statistically based correlations between the response and the above described intrinsic and extrinsic characteristics (Detter et al., 2019, 2023; Lundstrom et al., 2007; Moore, 2000; Nicoll et al., 2006).

In traditional pulling test procedures, an artificial load is applied to the tree at a given height on the stem and increased monotonically until failure of the tree, which occurs either by stem breakage or by uprooting. The resulting key parameter, i.e., the overall tree resistance, is translated by most wind damage risk models and Decision Support Systems (Ancelin et al., 2004; Gardiner et al., 2008, 2000; Peltola et al., 1999) into a Critical Wind Speed value, i.e., the wind speed that – through a mechanism of stress transfer via the drag on the tree canopy (Raupach, 1995, 1994, 1992) – would produce the same resulting moment on the tree. The analogy between static tree pulling tests and the action of wind on trees is particularly true when, during a strong wind phenomenon, a single major wind gust hitting the tree produces so much momentum that the tree is unable to dissipate the incoming input energy. Therefore, once the peak resistance is reached, the collapse of the system occurs inevitably.

However, it is known that in most strong winds (Gardiner, 2021), the wind's action on trees operates as a fluctuating load (Quine et al., 2021). In wind damage risk models, this is normally described by the gustiness, namely a ratio of the extreme to mean wind loading on trees (Gliksman et al., 2023). In artificial experiments, the tree is cyclically loaded with a force that can be applied with constant or variable amplitude. The rate of the force can be very important because pseudo-static approaches involve slow loading rates but can produce high input forces and non-linear response (e.g., O'Sullivan and Ritchie, 1993). High-rate loads are generally obtained at the expense of smaller amplitude forces, but the correct frequencies may place the tree under resonance. This might promote large deformations while preserving the global response within the elastic field (e.g., Rodgers et al., 1995) but the tree system might become fatigued (Gardiner et al., 2019; Leigh, 2014). However, recent work has demonstrated that tree response to the wind, at least for trees in forests, is a quasi-static process with trees responding to each gust during the storm without any enhancement due to resonance (Schindler & Mohr, 2019). Moreover, whilst these sequences of gusts have the potential to significantly damage trees, they may not provoke their complete failure, as observed by Nielsen (2011). He reported reduced rooting strength of surviving trees after a storm. Also Kamimura et al. (2022) observed residual damage to trees caused by a hurricane by comparing the lean angle of surviving trees before and after a storm.

All these concepts have been incorporated in several dynamic forest landscape models to introduce wind disturbances in simulated forest landscapes, allowing to investigation at the landscape scale how the size and the pattern of a disturbance event are influenced by forest management (Chen et al., 2018; Seidl et al., 2014).

There is extremely scarce and fragmented evidence in the literature about the response of trees subjected to repeated loads, i.e., cyclic loads. Rodgers et al.(1995) used a vibrodyne attached to a tree trunk to observe larger induced tree resonances and displacements to assess the frequency at which hydraulic fracturing of water-saturated soil reduces root anchorage stiffness. Jonsson et al. (2006) conducting two successive pull tests on five softwood trees found that the secant stiffness, i.e., the parameter that describes the amount of force required to produce a reference rotation of the tree, decreased significantly. Leigh (2014) combined experimental data and computational techniques to observe that trees could be subject to stem breakage due to low cyclical failure under repeated loading by high cyclical loads related to hurricane-force winds. Detter et al. (2019) performed pseudo-static cyclic pulling experiment on thirteen small-diameter broadleaf trees with increasing stem base tilt angles. This was done to assess whether the validity of the well-known curves predicting load tip also extends to repeated cycle loads (Wessolly, 1996). Václav et al. (2021) applied three subsequent cycles to ten different oak trees but keeping base rotation below 0.25°, which corresponds to the conventional elastic response threshold used in stability assessment techniques (Wessolly and Erb, 1998).

In static tests, tree pulling outcomes are normally evaluated through the derivation of applied moment vs. base rotation (M-θ) curves based on a classical equilibrium approach. It can be argued that the introduction of a cyclical test procedure could lead to a transition towards a type of analysis based on an energetic approach. In this case the wind-tree interaction may be evaluated also from a kinematic point of view in which the energy transfer may occur in subsequent steps. Additionally, this approach is already a standard procedure in studies dealing with the capacity of trees to form a barrier against rockfalls (Dorren and Berger, 2006; Lundstrom et al., 2009; Stokes et al., 2005).

This work aims to provide initial insights into of the biomechanical response of shallowly rooted Norway spruce growing in mineral soils and subjected to repeated increasing pulling loads up to tree failure. The mechanical behaviour of the tested trees is analysed by means of a classic equilibrium approach through the calculation of peak applied loads, stem base rotation, and the trend in equivalent stiffness over subsequent cycles and residual rotations. Tree biomechanics is also analysed via an energetic approach centred around energy absorbed and dissipated within either the single load cycle or the complete cyclic test, by applying standard procedures employed in the field of mechanical engineering. The main outcomes of the present work shall provide a starting point for the development of a novel characterisation of tree resistance to the wind as an alternative to destructive experiments, especially when it is important to consider the impact of repeated loads on trees.

2. Materials and methods

2.1. Site and trees description

The experimental tests were conducted in August 2021 in an even-aged Norway spruce forest in the Cansiglio forest (46°05'20.7"N 12°26'57.2"E, altitude = 980 m) in the north-eastern Italian Alps. Average yearly cumulated precipitation and solar radiations are 1100 mm and 3100 MJ/m^2, respectively. This site has been used in the past for similar studies (Marchi et al. 2019, 2022). Tests were conducted on a gently sloping terrain (5–10°), as opposed to the previous studies of Marchi et al. (2019) and Marchi et al. (2022), whose experimental sites were on flatter and more sloping terrains, respectively. The predominant soil groups include Epileptic Calcaric Phaenozem of limited depth (< 0.75 m) on limestone and marlstone bedrocks. The forest presented a homogeneous and regular structure with tree Diameter at Breast Height (DBH) values varying between 25 cm to 70 cm and an average tree height of 30 m. Six Norway spruce trees, with an average DBH of 35 cm, were randomly selected, and pulled. No edge trees were included in the pulling tests, in order to test trees with comparable crowns sizes.

2.2. Instruments and measurements

The same equipment used in the previous tests campaigns was employed (see Marchi et al. (2019) for a detailed description of the setup). Before each pulling test, cable height, cable vertical inclination, and azimuth of the pulling force were recorded, as well as the azimuth of the lateral roots. The applied pulling forces were recorded by means of a load cell applied to the pulling system. The rotation of the tree root-plate (i.e., the controlling parameter for the cyclic loading protocol) was monitored with a biaxial inclinometer (*Beanair GmbH, Berlin, Germany* model *WILOW-WIFI-HI-INC-30B*), with a range of ±30° and repeatability of ±0.004°. Tree-pulling forces and root-plate rotation data were transmitted in wireless mode to a logging laptop and recorded with BeanScape® Wilow® Basic software. A pair of clamp-type strain transducers (*Hottinger Brüel & Kjaer GmbH,* Darmstadt, Germany, model *DD1*) mounted on a 250 mm extension were connected to a Data Acquisition Module (*Hottinger Brüel & Kjaer GmbH,* Darmstadt, Germany, model *Quantum X MX840B*) to monitor the elastic strains on the outer fibres of the trunk. These data were recorded on the logging laptop with Catman®Easy software.

Due to the unreliable tree response when approaching near failure conditions, strain sensors were removed from the stem after measured peak rotations up to 2.0–4.0° to prevent damage to the equipment during the tree fall. The real-time wireless inclinometer was also removed once clearly visible permanent displacements of the tree were observed. In order to collect the rotation data during the complete overturning of the tree, a triaxial accelerometer with integrated datalogger (*Gulf Coast Data Concepts LLC, Waveland, MS, USA,* model *X2–2*) was secured to the tree base, protected by a waterproof canister.

2.3. Test procedure

The lack of cyclic tests on full standing trees in the literature prompted the design of the specific loading protocol used in the present study. Standard cyclic procedures for testing materials or engineering structures generally consist of displacement-based or rotation-based protocols. In this context, when the aim is to analyse fatigue-related phenomena, a given controlling variable (e.g., load or displacement amplitude) is maintained constant in each repetition O'Sullivan and Ritchie (1993) to detect any decrease in the observed mechanical properties (e.g., strength of the material). Such tests normally start in the elastic field of work of the element and may later be extended to the non-linear response field. Alternatively, in cyclic tests aimed to replicate phenomena characterised by irregular loading history (e.g., earthquakes or wind actions) a sequence of loads of increasing amplitude is applied to allow analysis of both the elastic and inelastic response of the tested element.

If the expected response is highly non-linear, the loading sequence is normally built up over a reference displacement threshold (i.e., the elastic limit) to analyse both the elastic and inelastic parts of a typical force vs. displacement curve. Once the threshold has been determined, e.g., by preliminary monotonic tests, repetitions with increasing displacement/rotation values are applied up to the failure of the tested element (Detter et al., 2019). The rate at which displacements are increased also depends on the expected non-linear response. Normally the aforementioned threshold correspond to the value below which elastic responses are assured independently from the number of loading cycles.

In the present work, we opted to perform the tests by progressively increasing the applied peak rotation at each step. This was done due to the complexity of applying high loads at a constant rate with an indirect pulling system, while attempting to mimic the nature of tree responses during a windstorm where the lean of trees subjected to high quasi-static wind loads and high dynamic wind loads (i.e., a quick succession of gusts) increases progressively (Jackson et al., 2021; Kamimura et al., 2022; Schindler and Kolbe, 2020).

Definition of the elastic limit in a tree-pulling experiment may not be as clear as with traditional materials testing. Regarding the root-plate rotation, an inclination of 0.25° is a threshold assumed in urban forestry (Wessolly and Erb, 1998). Whereas if strains of external wood fibres of the stem are also measured, then elongations up to 100 μm are taken as reference value. Recent studies on Norway spruce (Lundström et al., 2007; Marchi et al., 2019) indicated that angles up to 0.5° do not impede a total recovery of the rotation. As a consequence, 0.5° of rotation and 200 μm of strain were taken as the reference elastic limits for this work.

Two slightly different protocols were used. For the first two test trees, six repetitions were performed with almost constant rotation values corresponding to the elastic limit, and then rotation amplitudes were progressively increased until failure (Fig. 1). For the four remaining trees, repetitive loads at 0.5° were not undertaken in order to focus in the non-linear response of the tree when development of irreversible damage occurs (i.e., permanent stem base rotations).

2.4. Data processing and analysis

The post-processing analysis of the different data inputs was performed in Matlab® (The MathWorks Inc., 2023). The raw measurements from the sensors attached to the tree and the load cell were firstly synchronized via time stamps converting the three accelerations into corresponding biaxial rotation measurements. Signals were all resampled at a constant rate of 50 Hz. Measurements obtained from the inclinometer and the extensimeters were filtered with a moving average algorithm with a 2-second window length. Signals obtained from the accelerometers were provided with a slightly stronger filter namely, a Gaussian-weighted moving average filter having a smoothing factor of 0.001. This was done to identify the cleanest moment vs. rotation relation in order to produce a smooth visualisation of the hysteretic loops.

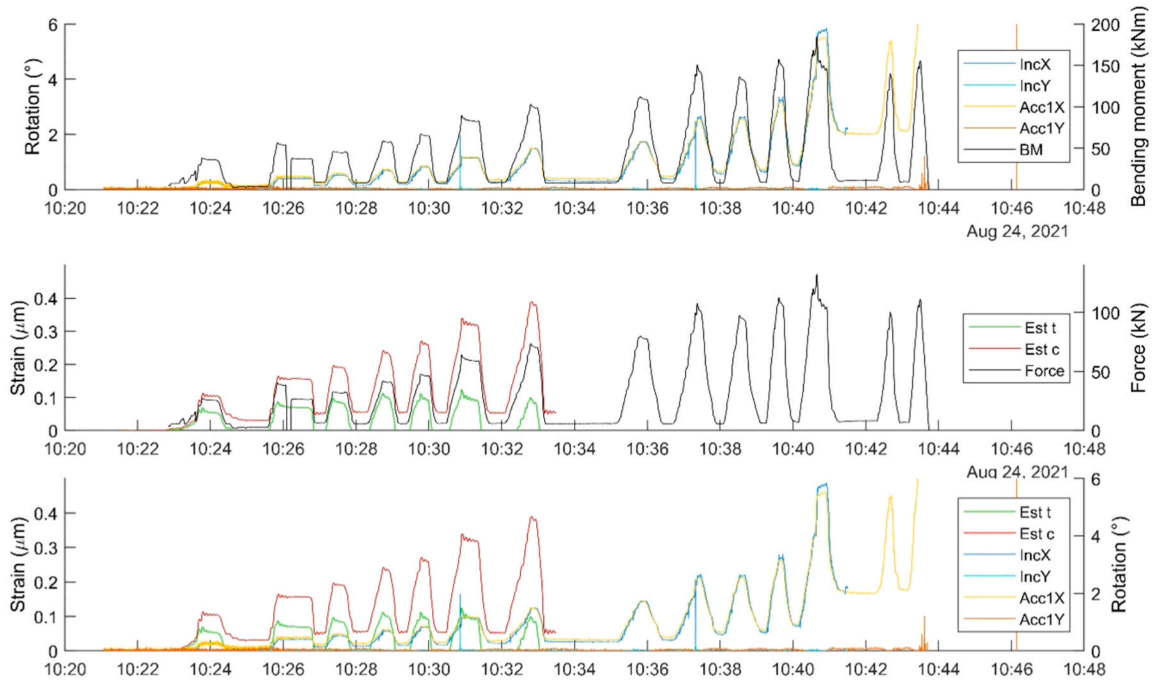

Fig. 1. Synchronized data from the equipped sensors for an exemplary tree (Tree C4): IncX, IncY, Acc1X and Acc1Y indicate tree rotation on the X and Y axes as measured by the inclinometer and accelerometer respectively; BM is the bending moment; Est_t and Est_c are the wood strains in tension and compression; Force is the measured force on the pulling cables.

2.4.1. Equilibrium (M-θ) approach

Monotonic pulling tests are normally analysed through synchronized timeseries of applied moment vs. rotation of the root-plate (M-θ), from which parameters such as the peak applied moment to the tree (M_{Peak}) and its corresponding rotation ($\theta(M_{Peak})$) can be extrapolated. Details on the mechanistic model employed to extrapolate these parameters are available in Marchi et al. (2022). M-θ curves may be also represented in non-dimensional terms (M_0-θ_0) by normalising the values of the applied moment (M) and the corresponding root-plate rotation (θ) by the respective maximum values of each variable extracted at the time of M_{Peak}, where $M_0 = M/M_{Peak}$ and $\theta_0 = \theta/\theta(M_{Peak})$.

In a cyclic loading test, the sum of subsequent load cycles defines the final response, and therefore the contribution of each single load cycle is important and must be carefully analysed (Fig. 2). Hence, the analysis was conducted from a structural point of view taking each i^{th} load cycle as a single observational unit. Firstly, the coordinates of the minimum ($\theta(M_{Min,i})$; $M_{Min,i}$) and maximum ($\theta(M_{Max,i})$; $M_{Max,i}$) points of the M-θ curve were extrapolated. The resulting line that connects all the peak values, normally referred as the "backbone" curve (i.e., the envelope curve) of the test, provides a first glimpse of the cyclic response. For common materials and structural systems, it is not possible for the backbone curve to be higher than the curve obtained from a monotonic test. Secondly, for each load cycle the secant stiffness $K_{S,i}$ (Eq. (1) and the reloading stiffness $K_{R,i}$ (Eq. (2) were estimated. The first parameter expresses the slope of the line connecting the origin of coordinates to the peak point (green line in Fig. 2). The latter is the slope of the line connecting the minimum and maximum points (blue line in Fig. 2).

$$K_{s,i} = \frac{M_{Max,i}}{\theta(M_{Max,i})} \tag{1}$$

$$K_{R,i} = \frac{M_{Max,i} - M_{Min,i}}{\theta(M_{Max,i}) - \theta(M_{Min,i})} \tag{2}$$

Comparing the slope of $K_{S,i}$ and of $K_{R,i}$ against the increasing $\theta(M_{max,i})$ provides information about irreversible damage occurring to the tree. The slope of the secant stiffness is a direct expression of how abrupt the shift to the non-linear response is, that occurs in the system. The slope of the reloading stiffness conveys information about the equilibrium conditions in which the tree is operating after each cycle. A constant trend may indicate only an accumulation of irreversible damage causing a shift of the initial conditions; a decreasing reloading stiffness may show that the mechanical response of the system (i.e., the root-plate system in this case) is being damaged during each cycle.

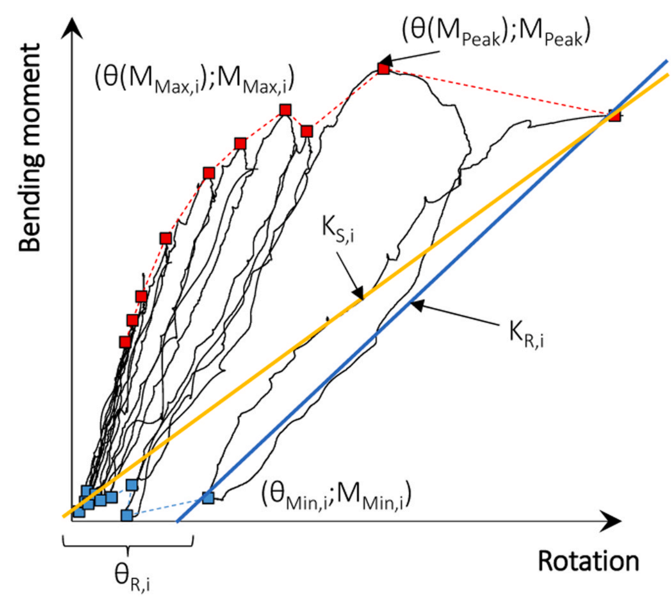

Fig. 2. Mechanical interpretation of a typical M-θ curve obtained from a cyclic test for an exemplary tree (Tree C3): backbone curve in dashed red; secant stiffness in yellow; reloading stiffness in blue. The red squares indicate the maximum applied moment and the corresponding root-plate rotation angle for each cycle 'i'. The blue squares indicate the corresponding minima.

Finally, damage occurring in the root-soil system is also estimated for each repetition by evaluating the intercept of $K_{R,i}$ with the x-axis (rotation), and expressed by the rotation $\theta_{R,i}$ occurring at the tree base after an applied moment corresponding to $M_{Peak,i-1}$. This ensures that $\theta_{R,i}$ can be correctly approximated even if some residual load is present at the end of the unloading phase (i.e., $M_{Min,i} > 0$), which depends specifically on the pulling system employed in the test.

2.4.2. Energetic approach

Another consolidated methodology for the analysis of cyclic tests involving non-linear responses is the energetic approach. When applied to a biological system like a tree, the input energy incoming from an external dynamic excitation (referred also as input work) is absorbed and then released (i.e., dissipated) throughout different phenomena. A root-soil interaction and friction within the wooden fibres of stem, branches, and roots are the main internal damping mechanisms whereas aerodynamic drag of the crown and collisions with neighbouring trees are examples of external damping mechanisms (Moore and Maguire, 2004; Spatz and Theckes, 2013). Breakages occurring at any levels are also a clear form of energy dissipation. Traditional destructive tree pulling tests can be assigned to the branch of tests involving "quasi-static loading conditions" rather than tree sway tests for which dynamic (namely, time-varying in this case) forces are introduced. Therefore, all the energy transfer and dissipation related to crown drag can be neglected in traditional destructive tree pulling tests.

Data analysis for the energetic approach can be performed similarly to the M-θ approach, taking the i^{th} load cycle as single observational unit (Fig. 3). In general, within each load cycle, all the input energy $E_{Input,i}$ (or external work W_i) generated by the application of any forces to the tree must be balanced by an equivalent amount of energy that has to be released once the load is completely removed. In a typical non-linear response, the output energy can be split into its elastic $E_{El,i}$ and inelastic (dissipated) $E_{Dis,i}$, components, thus leading to Eq. (3):

$$W_i = E_{Input,i} = E_{El,i} + E_{Dis,i} \tag{3}$$

Accordingly, in the hypothetical case of a completely elastic tree response to the external input energy, at the end of each load cycle when the force is released, $E_{Dis,i}$ is null, and $E_{Input,i} = E_{El,i}$. Irreversible deformations such as those occurring at the root-soil interface (e.g., due to root breakage, soil compaction, or other failures) result in $E_{Dis,i} > 0$.

The maximum input energy per load cycle $E_{Max,i}$ can be calculated according to Eq. (4) as the integral of the applied moment over the variation of rotation generated by that same moment (i.e., calculated between the minimum $\theta_{Min,i}$ and maximum $\theta_{Max,i}$ base rotations observed in the i^{th} load cycle):

$$E_{Max,i} = \int_{\theta_{Min,i}}^{\theta_{Max,i}} M(\theta)d\theta \tag{4}$$

The inelastic, dissipated energy per load cycle $E_{Dis,i}$ can be likewise calculated (Eq. (5)) taking into account in addition the release phase of the load, i.e., deducting the elastic component of the motion described by the rotation returning back from $\theta_{Max,i}$ to the value $\theta_{Min,i+1}$.

$$E_{Dis,i} = E_{Max,i} - E_{El,i} = \int_{\theta_{min,i}}^{\theta_{min,i+1}} M(\theta)d\theta \tag{5}$$

Alternatively, $E_{Dis,i}$ corresponds to the difference between the residual energy ($E_{Res,i}$) obtained at the end of two subsequent cycles (see Eq. (6) and (Fig. 4)):

$$E_{Dis,i} = E_{Res,i} - E_{Res,i-1} \tag{6}$$

With this evaluation, it is therefore possible to obtain an objective quantification of the actual energy absorbed and released, quantifying the damage occurring at the root-soil level during each cycle, and relating them to the total input work required to provoke complete overturning $E_{Max,Peak}$. Lastly, substituting the lower bound of integration with the first load cycle produces the total cumulative input energy $E_{Max,c,i}$ (see Eq. (7)) which is a useful parameter to analyse the contribution of each load cycle in the global response.

$$E_{Max,c,i} = \int_{0}^{\theta_{Max,i}} M(\theta)d\theta \tag{7}$$

Furthermore, the total absorbed energy was calculated at fixed steps of stem base rotation. Maximum energy inputs were computed at M_{Peak}, to evaluate the total energy applied to the tree to provoke its overturning. Similarly, values of E_{pot} were calculated also for the pulling tests performed in the same test site (see Marchi et al. 2019, 2022) and results compared with the ones obtained from this study. Simple linear regressions were also computed with the different datasets to detect whether a relationship with typical allometric tree volume predictors

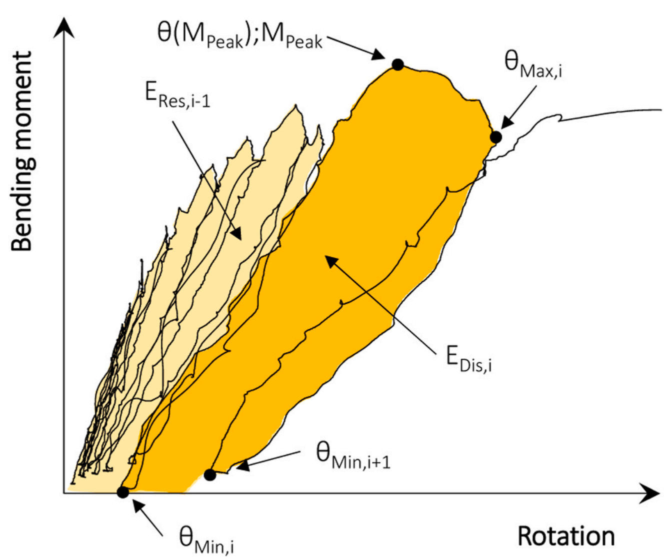

Fig. 3. Energetic interpretation of a typical M-θ curve obtained from a cyclic pulling test for an exemplary tree (Tree C3): area shaded in orange corresponds to $E_{Dis,i}$ as defined by the integral in Eq. (5) relative to the i-th cycle; area shaded in light yellow is defined as the residual energy $E_{Res,i-1}$ up to the i-1 cycle;.

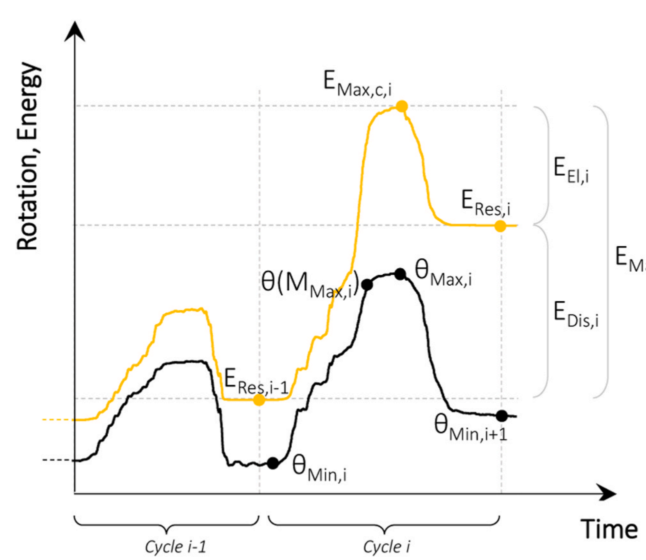

Fig. 4. Time-series with rotation (in black) and corresponding energy (in orange) values. Dots represent the characteristic points of each load cycle. The magnitude of the different energy components $E_{Max,i}$, $E_{Dis,i}$, $E_{El,i}$ and $E_{Res,i}$ and the corresponding rotations under which they are evaluated $\theta_{max,i}$ to the value $\theta_{min,i+1}$ are also reported.

could be an explanatory variable for the total dissipated energy.

3. Results

3.1. Test protocol

The loading protocol was successfully applied on all six trees of which DBH and Height were given in Table 1. The testing environment and the unpredictable response of the trees once they experience large non-linearities did not allow the application of a uniform loading rate during the whole test as is normally achieved in a controlled environment such as a laboratory. Each test required between 30 and 60 minutes for the complete execution depending on the total number of load cycles and comprised between ten (tree C3) and sixteen (C6) load repetitions characterised by different rotation amplitudes $\theta(M_{Max,i})$ with a minimum of 0.2° and a maximum of 5.7° obtained in a post-peak phase (Table 1 and Fig. 5a). Limiting the analysis to the pre-peak load cycles, the one-step rotation increment $\Delta\theta$, namely the difference of rotation values between two consecutive peaks, varied between 0° to 2.2° with a non-uniform pattern obtained between the tests (Fig. 5b). For smaller values of θ, the rotation increments $\Delta\theta$ could be thoroughly controlled, while rotations above 1–2° resulted in a less predictable inelastic response of the tree causing inevitable higher jumps of $\Delta\theta$.

Observing the distribution of the peak points expressed in non-dimensional terms for each cycle (Fig. 6), the high concentration of load cycles performed with $\theta_0 \leq 0.2$ can be observed. However, a notable number of load cycles was also achieved with rotations up to $\theta_0 \leq 0.5$., i.e., half of the trees' rotational capacity before failure. In four cases, additional pulls could also be performed in the post-peak phase ($\theta_0 > 1$) for trees from C1 to C4 (see Fig. 6).

Fig. 6 also anticipates the trend of the non-dimensional curves obtained for the trees. Trees C1 to C4 have a similar behaviour, whereas tree C5 shows how near failure conditions were reached several times before the complete tree failure. The apparently unclear response of Tree C6 showing multiple values of M_0 within the same range of θ_0 is probably due to some load cycles being performed after partial damage of the root system.

3.2. Overall behaviour and hysteretic response

The hysteresis cycles obtained from the repeated pull and release procedure are notably different between the tested trees, Fig. 7.

The first sample, tree C1 (Fig. 7a) showed an almost perfectly linear response up to load cycle #4, indicating absence of damage to its anchoring system, i.e., the tree had the tendency to return to its original perfectly balanced position. The next five load cycles again provided almost the same response, although with a notable reduction of stiffness (details reported in the following section). Additionally, the same M-θ curve describes a very limited non-linear response for most of the load cycles showing a relatively more marked inelastic response only at the eleventh cycle, where about 80 % of M_{Peak} was applied (see also Fig. 6). Tree C1 also shows that upon reaching M_{Peak} the base rotation shifted from 2.96° up to about 6–7° before the self-weight of the tree started to overwhelm the overall stability producing an increase of rotation even after a reduction of the applied moment. To test the tree response in a highly displaced condition, load on the pulling system was immediately removed with the root-plate registering a rotation of 11.58°, almost four times $\theta(M_{Peak,i})$. At this point the applied moment was about a half of M_{Peak}. The complete release of load provoked a permanent rotation of 6.42°. In the successive final pull (load cycle #13) the tree was capable to withstand a peak moment of 64.83 kNm, i.e., 60 % of M_{Peak}.

A response to be highlighted is the one obtained from Tree C2 (Fig. 7b) were an elastic behaviour turned abruptly into an inelastic one and immediately reaches M_{Peak} at load cycle #7 with $\theta(M_{Max,i})$ increasing from 0.73° to 2.81° (+284 %). Four more pulls were performed in the post-peak phase. Three of which again almost produced an elastic response, and only one (load cycle #10) additionally damaging the tree anchoring capacity. The load cycle corresponding to the last pull (#12), the one leading to the complete overturning, is not plotted in Fig. 7b due to an error in the acquisition of the tensile forces.

Tree C3 (Fig. 7c) represents the case of a progressive accumulation of irreversible rotations occurring at the base, a phenomenon typically referred in structural engineering as "ratcheting". A decreasing trend of the reloading stiffness can be noticed, detailed in the following section, that describes an overall reduction of the global tree stability for subsequent loads. Additionally, the reduction in resistance that occurred between the fourth-last and third-last pull (load cycles #7 and #8) is notable, an evident sign of failure occurring to the root-soil plate system. Finally, the loop also shows how it was possible to apply an additional pulling cycle (load cycle #10) even after achieving the peak resistance M_{Peak}. In this case, the maximum moment decreased from 269.35 kNm to 241.44 kNm (-10.4 %) while base rotation $\theta(M_{Max,i})$ increased from 3.96° to 6.91° (+74.5 %).

Tree C4 behaved similarly to tree C3 showing again that after major damage. The sound of roots breaking could be clearly heard during the load cycles but could not be physically seen or inspected during the test. The drop in resistance could not be recovered in the following two pulls that were performed in the post-peak phase (load cycles #12 to #14) (Fig. 7c). In this case, the maximum moment $M_{Max,i}$ decreased from 185.24 kNm to 155.95 kNm (-15.8 %) while base rotation $\theta(M_{Max,i})$ increased from 5.29° to 7.72° (+45.9 %).

Tree C5, similarly to trees C3 and C4, returned a progressive increase of damage which already began from load cycle #3 where only 10 % of M_{Peak} was applied. The post-peak pulling phase, registered a maximum resistance of 96 % of M_{Peak} in load cycle #12, i.e., a resistance almost equal to the peak one, but producing a base rotation value of +43 %.

Tree C6 displayed a behaviour similar to that of tree C1 with the exception that evidence of irreversible residual rotations was observed (the several drops in resistance on the leftmost side of Fig. 7f). This test was characterised by the highest amount of load cycles (16), but all limited to the pre-peak phase and with $M_{Max,i}$ less than 62 % of M_{Peak}.

Although the tested tree samples provided very similar growing characteristics in terms of size, soil and weather conditions, it is interesting how the single cyclic response can change considerably. A possible explanation for the apparent random cyclic response of the tree could be due to the different stability components (Coutts, 1986) that intervene and act in a non-univocal manner. For example:

Table 1
Main parameters of the loading protocols of the cyclic pulling tests.

ID	DBH (cm)	H (m)	Total # of load cycles (dimensionless)	Cycles with $\theta_{Max,i} \leq 0.5°$ (dimensionless)	Cycles with $\theta_{Max,i} > \theta(M_{Peak})$ (dimensionless)	Average $\Delta\theta$ (°)
C1	38.5	29.0	13	5	1	0.24
C2	43.0	31.5	12	3	4	0.43
C3	41.0	30.5	10	0	1	0.56
C4	31.5	26.0	15	3	2	0.41
C5	40.0	30.0	13	3	3	0.51
C6	35.0	28.0	16	4	0	0.16

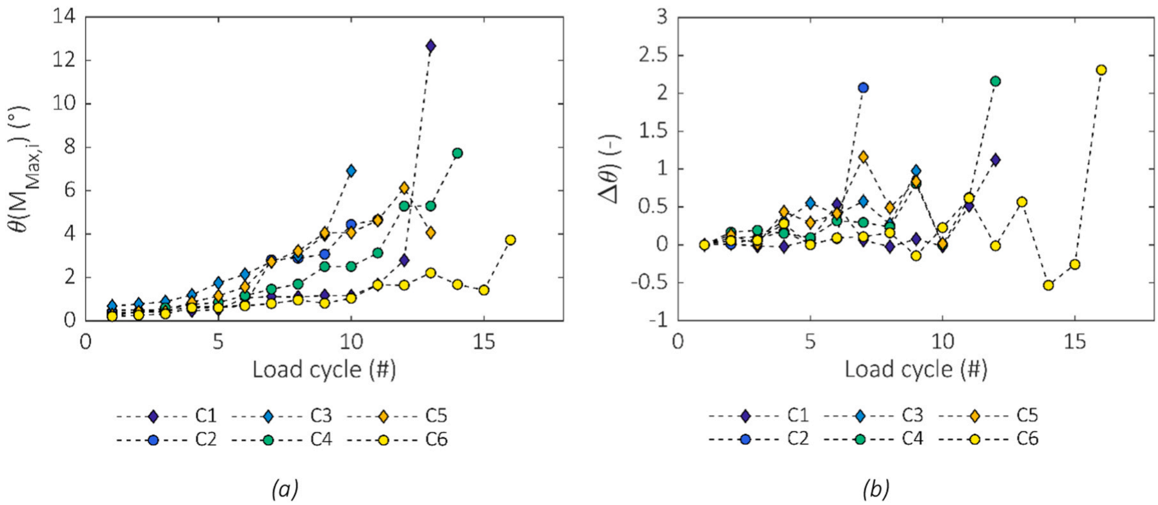

Fig. 5. Peak rotation $\theta(M_{Max,i})$ reached on each load step (a) and relative increment $\Delta\theta$ up to the peak cycle (b).

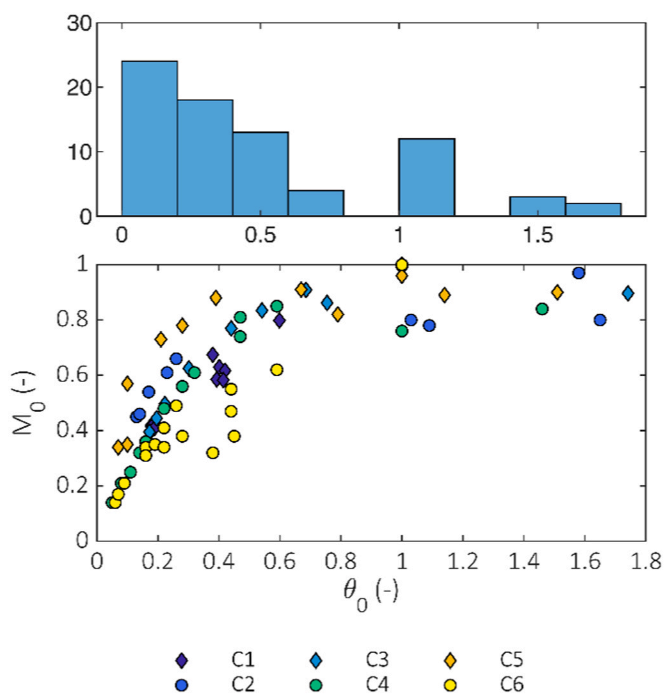

Fig. 6. Load cycle frequency distribution (top) and maximum M_0-Θ_0 reached on all load steps (bottom).

- a strong and rigid windward root system can initially overwhelm the other resisting mechanisms significantly, leading to a pure elastic response (e.g., tree C1) where the small stiffness reduction is only due to the damage expressed as a soil compaction in the leeward side of the root-plate;
- a windward root system not well aligned with the pulling direction may lead to an anticipated higher contribution of the soil component leading to higher irreversible deformations since the first repetitions (e.g., tree C3);
- a weak root system in the windward side may also lead to premature failures (e.g., tree C6) and to a redistribution of the bearing capacity to the remaining components (soil, leeward roots, etc.).

3.3. Equilibrium (M-θ) approach

3.3.1. Root-plate stiffness

Fig. 8 shows the calculated secant $K_{S,i}$ and reloading stiffness $K_{R,i}$ vs. base rotation $\theta(M_{Max,i})$. To perform a direct comparison between the different tests results, the ratio $\chi = K_S/K_R$ is also plotted against the non-dimensional rotation $\theta_{Max,i}/\theta(M_{Peak})$ (Fig. 9). The ratio varies between 0.5 and 1.1. Trees C1 and C3 had a positive decreasing linear correlation of χ with θ_0. This was confirmed by positive coefficients of determination ($R^2 > 0.55$), highlighting that the loss of overall stiffness was affecting more the rotations at the peak points $\theta(M_{Peak,i})$ than the increasing irreversible rotations once the loads were at the minimum $\theta_{R,i}$. For the remaining trees, highly scattered data and general unclear trends ($R^2 < 0.10$) can be observed (Table 2). Tree C6 showed the lowest average χ of the tests (0.72). Damage concentrated in the first cycles. This suggested that some residual "damage" did initially occur to the tree. Its increasing trend proves that within the last cycles the root-plate managed to stabilize in a permanently deformed condition (with small increases of θ_R).

3.3.2. Residual rotations

The damage to the anchoring systems can also be deduced from the residual or irreversible rotations $\theta_{R,i}$ of the root-soil system limiting analysis to the pre-peak phase (Fig. 10). From the results, it emerges that in most cases the magnitude of $\theta_{R,i}$ was always below 20 % of the rotation at the peak moment (i.e., $\theta_{R,i}/\theta(M_{Peak}) < 0.2$) even for applied non-dimensional moment values M_0 approaching failure limits. It is also worth noting the different response between trees: as an example, Tree C1 shows almost no residual rotations, contrary to trees C3 and C4 which show increasing residual rotations related to the increasing magnitude of the applied moment. This was confirmed by testing the linear correlation between the applied moment $M_{Max,i}/M_{Peak,i}$ and the ratio $\theta_{R,i}/\theta(M_{Peak})$, which provided limited to no dependency in all cases ($R^2 < 0.45$, see Table 3). In the four tests where post peak pulls could be performed, the $\theta_{R,Peak+1}$ was on average 35 % of θ_{Peak} (see supplementary material).

3.3.3. Trends of parameters at peak points

To quantify the evolution of damage to the tree during testing, it was taken the load cycle for which M_{Peak} is registered as a reference and comparing the extrapolated mechanical parameters with the ones obtained from the previous and subsequent (if present) load cycles (Table 4).

The results for Tree C1 highlight again this tree's capacity to withstand remarkable loads even when starting from a significantly

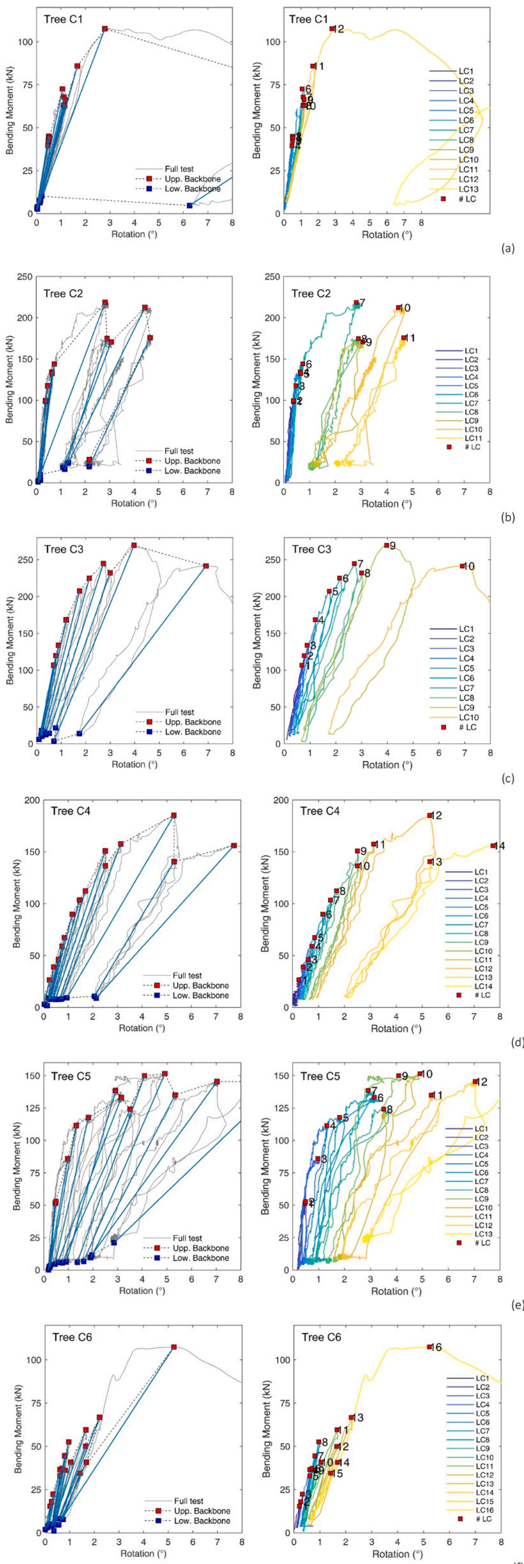

Fig. 7. Cyclic response of Trees C1 to C6 (a to f): M-θ loop (grey line); Upper and lower backbone curves and max point on each load cycle (red and blue markers); reloading stiffness for each load cycle (blue lines).

displaced condition ($\theta_{R,i} = 5.75°$). However, the calculated stiffness (K_R) after the peak was reduced to about one fourth of its original value. For tree C2, rotations values were also very limited until the pre-peak cycle ($\theta_{Max,Peak\text{-}1}$ /$\theta(M_{Peak})$ = 0.25) and serious damage was obtained only at the load cycle #7, when M_{peak} was achieved. This is confirmed by the sudden drops in the secant and reloading stiffness. Tree C3, C4 and C5 exhibit very similar mechanical responses up to the peak load cycle. However, in the post-peak load cycle Tree C3 achieved an $M_{Max,Peak+1}$ equal to 90 % of M_{Peak} at the expense of a drastically higher base rotation ($\theta_{Max,Peak+1}/\theta(M_{Peak}) = 1.74$). Conversely, in the post-peak load cycle Tree C4 only reached an $M_{Max,Peak+1}$ of 76 % of M_{Peak},without any changes in base rotation ($\theta_{Max,Peak+1}/\theta(M_{Peak}) = 1.00$). Tree C5 showed how two subsequent load cycles with extremely similar peak points could (Peak-1 and Peak in the corresponding C5 row of Table 2) be achieved. For Tree C6, load cycles #14 and #15 were not included in the analysis because they only displayed an elastic response (see the following section for details).

3.4. *Energetic approach*

3.4.1. *Cumulative energy*

The progressive cumulative dissipated energy was calculated from each available M-θ hysteretic loop up to the peak resistance M_{Peak}. The timeseries in which the computed cumulative dissipated energy is superimposed with the corresponding root-plate rotation (Fig. 11) provides an immediate overview of the difference in the energy dissipated demonstrated by each test. Most of the time lag occurring in the tests was removed to enhance clarity of the plots, thus obtaining a lower time than the "operative" one shown in Section 3.1. For Tree C1 (Fig. 11a) it is clear how the first five load cycles with rotation limited to 0.5° produced elastic responses, while the following five cycles performed at a constant amplitude of rotation $\theta_{Max,i} \approx 1.1°$ show a relatively small but increasing energy dissipation. Load protocol for Tree C3 (Fig. 11b), consisting of a constantly increasing value of $\theta_{Max,i}$ up to 3°, caused a parallel increasing energy dissipation which progressively continued in later load cycles. Conversely, Tree C4 (Fig. 11c) shows that elastic responses were achieved with base rotations $\theta_{Max,i}$ up to 1.6°, i.e., much more than the usual expected limit of 0.25–0.5°. Only the load cycles that produced a base rotation of 2.5° showed residual energy which translates into the first instances of damage happening within the root-soil system. The pulling procedure of Tree C6, characterized again by increasing values but with a more limited magnitude than the previous tests ($\theta_{Max,i}$, < 1° at load cycle #10), showed minor energy dissipation at 0.6°, and the greatest contribution started only for $\theta_{Max,i}$, above 1.0°.

3.4.2. *Trends of dissipated energy up to peak resistance*

The impact of each load cycle in terms of energy dissipated against the input work applied to the tree can be seen in Figs. 12 and 13 in the form of three different ratios plotted against the non-dimensional peak rotations, and taking the load cycle as the single observational unit (as in the example shown in Fig. 3).

Plotting the residual energy over the cumulative input energy ($E_{Res,i}$/$E_{Max,c,i}$) and relating it to the non-dimensional rotations ($\theta_{Max,i}$/$\theta(M_{Peak})$) (Fig. 12a) shows how the irreversible rotations may produce high values of $E_{Res,i}/E_{Max,c,i}$ even at the very first cycles (see tree C3 and C6 in Fig. 11c,f and Fig. 7c,f). The opposite phenomenon can be observed for tree C1 and C4 (see Fig. 11a,d and Fig. 7a,d), where the low amounts of dissipated energy confirm the almost elastic behaviour of this tree in its first few cycles.

Considering the ratio between the energy dissipated $E_{Dis,i}$ and the maximum energy applied within each load cycle $E_{Max,i}$ generally showed a great variability, with values below 0.5 and only a limited amount of load cycles involving a totally elastic response ($E_{Dis,i} = 0$). Relating this ratio to the non-dimensional rotation provides no clear trends (Fig. 12b).

Finally, the values of the relationship between $E_{Dis,i}$ and the maximum work leading to the peak resistance $E_{Max,peak}$ decrease drastically with maximum values consistently lower than 0.10 (Fig. 13). The greatest registered damage (i.e., energy dissipation) obtained before overturning of any of the test trees was obtained at load cycle #7 of Tree C3 where 10 % of the maximum input work was dissipated. This clearly

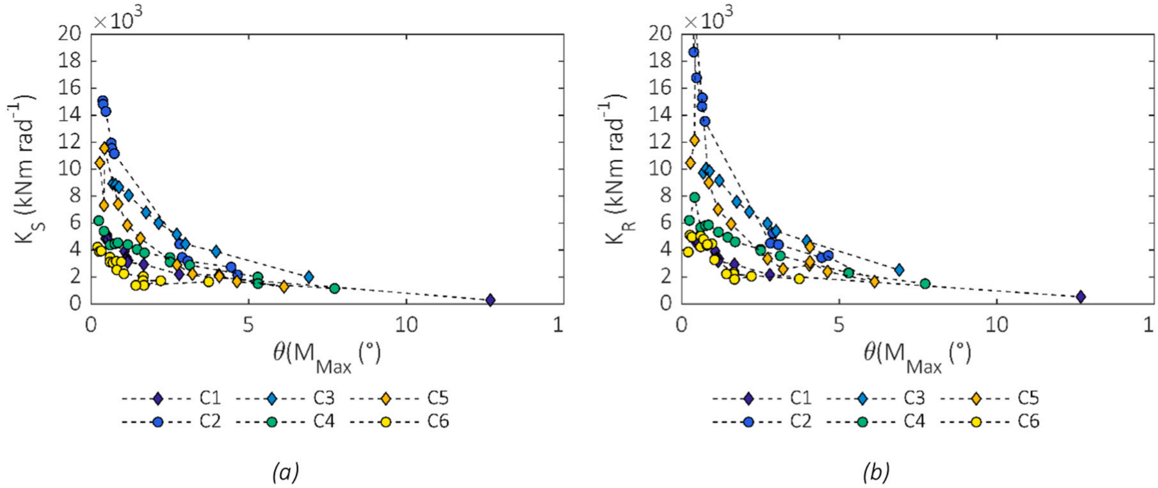

Fig. 8. Secant stiffness vs. rotation (a) and reloading stiffness vs. rotation (b).

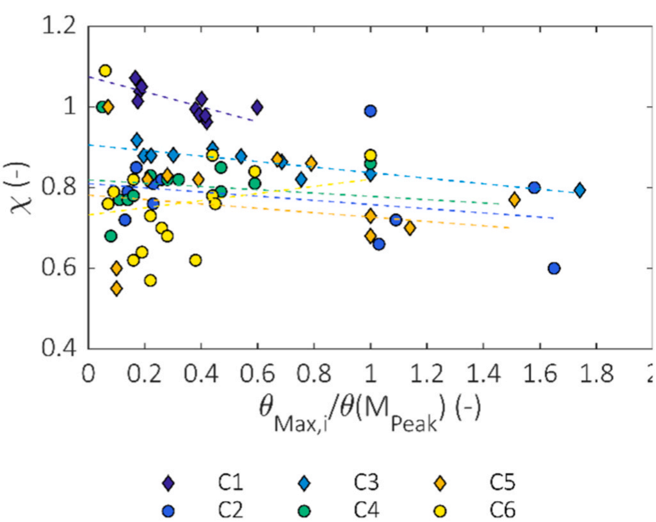

Fig. 9. Ratio of K_s/K_R vs. $\theta(M_{Max,i})/\ \theta(M_{Peak})$.

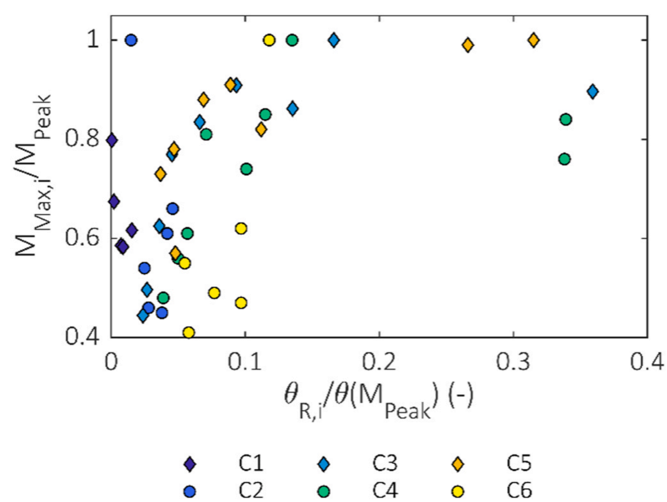

Fig. 10. Variation of the ratio $M_{Max,i}/M_{Peak,i}$ versus the residual rotation $\theta_{R,i}$ over $\theta(M_{Peak})$.

Table 2
Regression parameters of K_s/K_R vs. $\theta(M_{Max,i})/\ \theta(M_{Peak})$. Degrees of Freedom (DoF), Coefficient of determination (R^2), Root Mean Square Error (RMSE), Standard Error (SE) and P-value of the estimate.

ID	DoF	R^2	RMSE	Estimate	SE	P-value
C1	9	0.559	0.025	1.075	0.019	< 0.0001
C2	9	0.090	0.104	0.810	0.049	< 0.0001
C3	8	0.791	0.018	0.906	0.009	< 0.0001
C4	12	0.046	0.082	0.819	0.033	< 0.0001
C5	11	0.032	0.148	0.782	0.070	< 0.0001
C6	14	0.027	0.132	0.732	0.055	< 0.0001

Table 3
Regression parameters of $M_{Max,i}/M_{Peak,i}$ vs. $\theta_{R,i}$ over $\theta(M_{Peak})$. Degrees of Freedom (DoF), Coefficient of determination (R^2), Root Mean Square Error (RMSE), Standard Error (SE) and P-value of the estimate.

ID	DoF	R^2	RMSE	Estimate	SE	P-value
C1	9	0.331	0.122	0.548	0.037	< 0.0001
C2	5	0.146	0.188	0.798	0.207	1.19E-02
C3	8	0.421	0.175	0.594	0.077	< 0.0001
C4	12	0.411	0.221	0.408	0.081	2.80E-04
C5	11	0.441	0.175	0.623	0.072	< 0.0001
C6	14	0.327	0.173	0.204	0.089	3.71E-02

shows how only for non-dimensional rotations values $\theta_{Max,i}/\theta(M_{Peak}) > 0.40$ tangible damage can be observed for trees C3 and C4, while Trees C1 and C6 only displayed very limited damage within nearly the entire testing procedure.

3.4.3. *Allometric predictors for energy*

The same energetic approach was also applied to evaluate the response of the monotonic M-θ curves available including the results from the previous test campaigns. The datasets on flat (Marchi, 2019) and sloped terrain (Marchi et al., 2022) were treated as separated samples. Data originated from this work was included in the sloped terrain dataset. The cumulative energy $E_{Max,c}$ evaluated at different level of rotations was linearly correlated to the overturning moment M_{Peak} (Fig. 14) and to the stem volume predictor DBH^2xH (Fig. 15). Results shows very high correlation between energy and both tested variables regarding slope terrain. The same is valid using DBH^2xH as explanatory variable for the sloped terrain condition but not for the flat terrain. Here the greater dispersion ($R^2 < 0.43$) is found in all intermediate values of θ, with except of $\theta(M_{Peak})$ were a $R^2 = 0.78$ is obtained. Therefore, a prediction of the cumulated energy at overturning $E_{Peak,c}$ can be quite reliably estimated starting from both M_{Peak} and DBH^2xH.

Table 4
Main parameters describing pre-peak, peak and post-peak load cycles.

ID	Cycle #	Description	$\theta(M_{Max,i})$ (°)	$M_{Max,i}$ (kNm)	$M_{max,i}/M_{peak}$ (dimensionless)	$\theta(M_{Max,i})/\theta(M_{Peak})$ (dimensionless)	$K_{S,i}$ (kNm/rad)	$K_{R,i}$ (kNm/rad)	$\chi_{,i}$ (dimensionless)	$\theta_{R,i}$ (°)	$\theta_{R,i}/\theta(M_{max})$ (dimensionless)
C1	11	Peak - 1	1.67	85.90	0.80	0.60	2941	2944	1.00	0.00	0.00
	12	Peak	2.80	107.61	1.00	1.00	2205	2166	1.02	-0.05	-0.02
	13*	Peak + 1	12.66	64.83	0.60	4.53	293	537	0.55	5.75	2.06
C2	6	Peak - 1	0.74	140.02	0.65	0.25	10,856	13,344	0.81	0.14	0.05
	7	Peak	2.94	214.65	1.00	1.00	4183	6644	0.63	1.09	0.37
	8	Peak + 1	2.93	170.88	0.80	1.00	3342	5199	0.64	1.05	0.36
C3	8	Peak - 1	3.00	232.13	0.86	0.75	4441	5412	0.82	0.54	0.14
	9	Peak	3.97	269.35	1.00	1.00	3888	4662	0.83	0.66	0.17
	10*	Peak + 1	6.91	241.45	0.90	1.74	2001	2521	0.79	1.43	0.36
C4	11	Peak - 1	3.13	157.47	0.85	0.59	2881	3578	0.81	0.61	0.12
	12	Peak	5.29	185.24	1.00	1.00	2006	2320	0.86	0.72	0.14
	13	Peak + 1	5.30	140.49	0.76	1.00	1520	2296	0.66	1.79	0.34
C5	9	Peak - 1	4.05	149.88	0.99	1.00	2119	2891	0.73	1.08	0.27
	10	Peak	4.07	151.78	1.00	1.00	2138	3121	0.68	1.28	0.32
	11	Peak + 1	4.63	135.02	0.89	1.14	1671	2404	0.70	1.41	0.35
C6	13	Peak - 3	2.22	66.76	0.62	0.59	1725	2031	0.84	0.34	0.10
	16*	Peak	3.73	107.46	1.00	1.00	1650	1872	0.88	0.44	0.12

* Cycle number corresponding to the tree overturning.

4. Discussion

Experimental cyclic pulling tests were performed on six Norway spruce trees by performing a sequence of pull and release cycles up to the peak resistance of the tree and even beyond that value in some cases. With reference to the whole existing dataset, 43 trees in total (Marchi et al., 2023), the dimensions of the trees tested cyclically fit nearer the lower bound of the dataset with an average DBH of 35 cm.

The applied loading protocol involved quasi-static loading conditions, that well simulate the medium-term strong wind condition, where subsequent gusts of wind hit the trees without inducing resonance (Schindler and Mohr, 2019, 2018). In this regard, the pulling procedure was also easier to design and quickly replicate on a number of specimens as opposed to a real dynamic loading test, which would still require that an apparatus such as a vibrodyne be firmly installed on the tree (Rodgers et al., 1995). Furthermore, it is still unclear and far from accepted whether the amplitude of these simulated gusts should be kept constant, thus simulating some oligo-cyclic fatigue phenomena (Leigh, 2014), or ramped, thus reproducing an increasing energy input. Wind gustiness is known to be affected by surface roughness, wind speed and height above ground (Gardiner et al., 2016; Gliksman et al., 2023) but it is difficult to translate the time series of a windstorm into a discrete number of gusts that can be confidently expected to strike a tree. In addition, it should be noted that the pulling system used was not able to precisely control the maximum allowable trunk displacement (and therefore base rotation) on each load cycle as in O'Sullivan and Ritchie (1993). Whilst in their study a more complicated and effective system was employed, it was in fact applied to trees felled at a height of 1.5 m. Therefore removing the stabilizing contributions of the tree crown and of large portions of the stems, and therefore not being able to fully account for a tree's overall stability.

In previous test campaigns (Marchi et al., 2022, 2019), tree failure was primarily observed as uprooting, which is typical of shallow-rooted trees (Blackwell et al., 1990; Coutts, 1986). In the present study, each test involved between ten and sixteen load cycles, producing some clear non-linear hysteretic loops once the trees' responses deviated from elastic. In four out of the six tests, additional pulls were also performed in the rather unexplored field of the post-peak phase, i.e., when the root-soil plate of a tree was already quite severely damaged. But the tree self-weight was not yet overwhelming the residual anchoring capacity. The post-peak pulls demonstrated that leaning angles well above the values corresponding to the peak resistance could be achieved without complete tree overturning. This confirms what can be observed after strong wind events (e.g., Kamimura et al., 2022; Nielsen, 2011). In these cases, a remaining resistance between 60 % and 90 % of the M_{Peak} was registered before complete failure was finally achieved. It is to be noted that the long-term stability will remain compromised and very these trees seldomly recover.

Whilst the number of samples in this study is low (six trees), the very similar tree size allows a robust stiffness analysis to be performed. Two different behaviours could be extracted from the tests. The first shows a complete equivalence between secant and reloading stiffness even after peak loads produced rotations above 1.0°, which translates into a system still working elastically (as reported in other field studies, e.g., James et al., 2013) but with a potentially consistent stiffness reduction observed in the cycle corresponding to M_{Peak} (e.g., a ~33 % reduction for tree C1). The second shows an accumulation of small irreversible base rotations occurring right after the initial cycles with a reloading stiffness higher than the secant one. This leads to a reduction of overall stiffness with a combined progressive increment of the root-plate tilt after each load repetition.

The sequence of loads produced progressive irreversible rotations of the tree root-plate as already evidenced in studies about the stability of anchor trees in cable logging activities by Marchi et al. (2021, 2020). This phenomenon has also been described as relaxation in some non-destructive (James et al., 2013) and destructive cyclic pulling tests (Detter et al., 2019; O'Sullivan and Ritchie, 1993). Although the magnitude of these residual deformations was limited in all tested trees (below 20 % of $\theta(M_{Peak})$ in our case), these results provide valuable insight into the different responses to wind dynamic excitations in detailed simulations that include root hinge stiffness as a parameter (Neild and Wood, 1999).

The average residual base rotation $\theta_{R,i}$ measured after the peak load cycle was ≈1.6° (35 % of $\theta(M_{Peak})$) with the exception of one case in which the tree was tilting with a base angle of 6.2°. This yields two scenarios. In the first one, it is possible that trees not showing particularly evident damage after a windstorm, aside from a deviation of their stem from the vertical might already have suffered considerable damage, as observed by Kamimura et al. (2022). In these cases, if sufficient recovery time is not available to the tree, any subsequent windstorm even of low magnitude may cause the survivor trees to ultimately collapse (Nielsen, 2011). Similarly, heavy snow loads not associated with particularly high wind speeds might also lead to tree failure, although the most common mode of failure in these situations appears to be stem breakage rather than whole tree uprooting (Nykänen et al., 1997; Peltola et al., 2000; Silins et al., 2000). In the second scenario

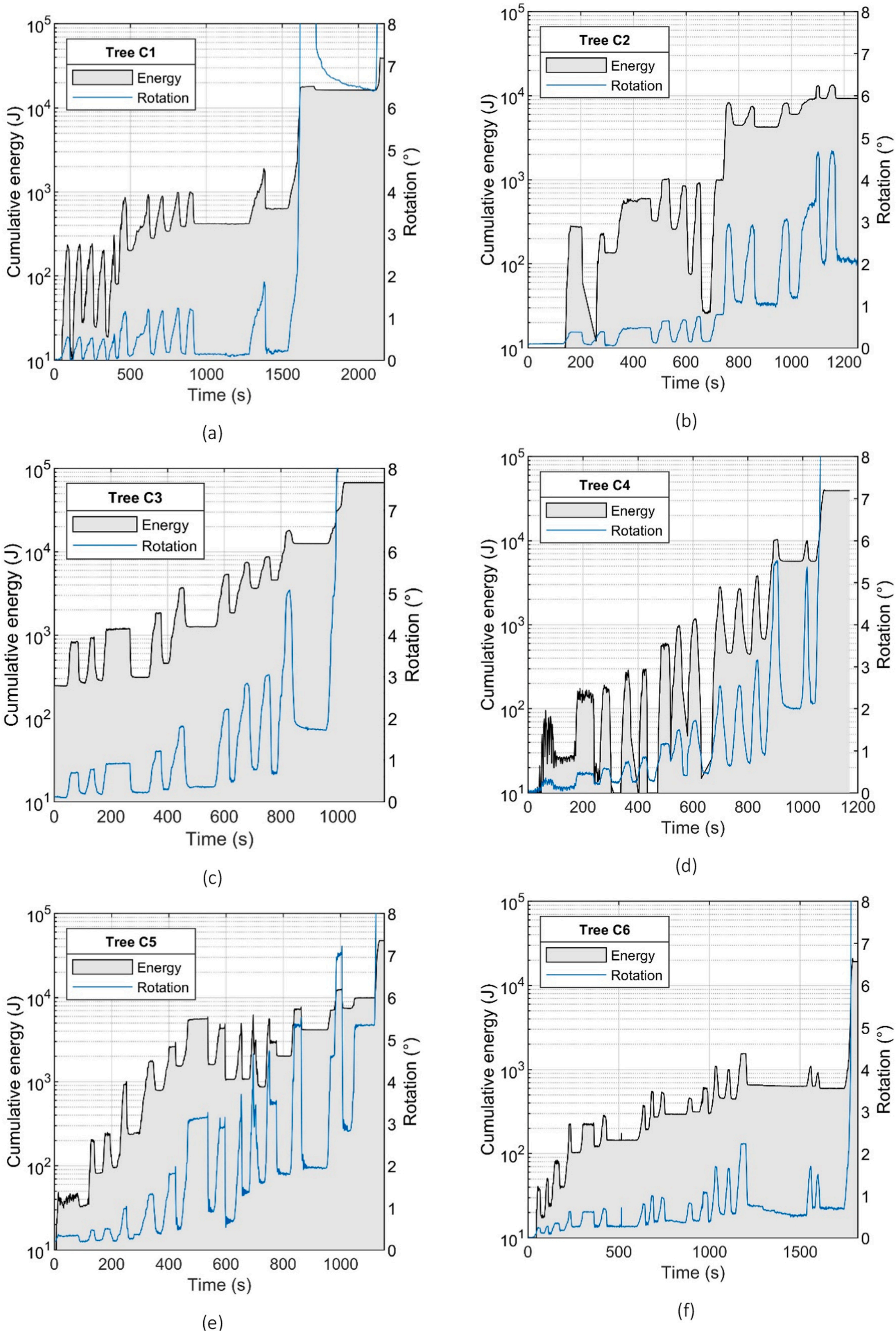

Fig. 11. Cumulative dissipated energy during the pulling test for all trees. Timeseries are limited to the load cycle before the tree overturning (therefore rotations on the right y-axis are limited to 8° to improve viewing clarity).

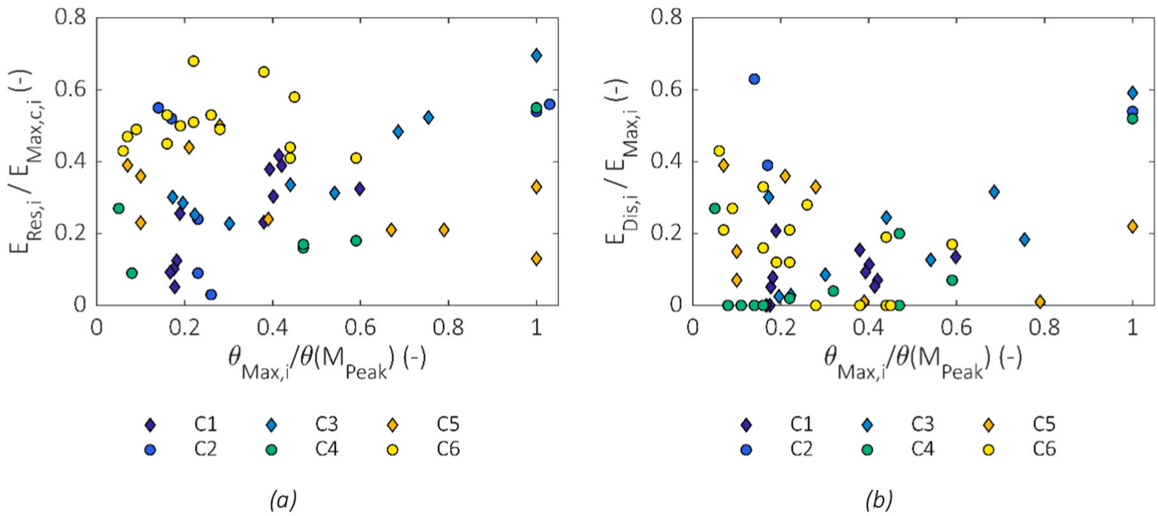

Fig. 12. Ratio $E_{Res,i}$ /$E_{Max,c,i}$ vs. normalised maximum rotation (a); Ratio $E_{Dis,i}$ /$E_{Max,i}$ vs. normalised maximum rotation (b).

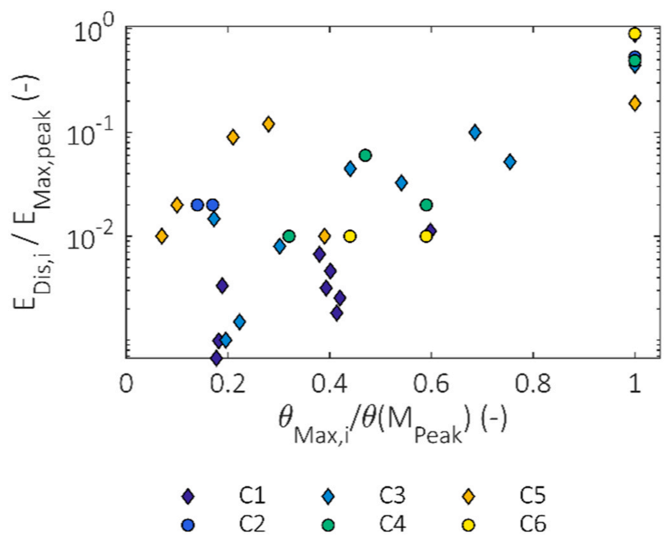

Fig. 13. Dissipated energy in relation to maximum energy input at peak resistance ($E_{dis,i}$ /$E_{Max,Peak}$) (in log-scale for clarity) vs. non-dimensional maximum rotation.

trees still possess some residual strength also at significantly displaced positions, which can be confirmed by the still standing, but leaning trees in forests affected by strong winds. However, this remnant anchorage strength is often fairly low in comparison to that of the initial, unperturbed state. Additionally it should be considered that as the tree leans towards the direction of the pull, these dislodged soil and rock debris are likely to drop from the soil-root plate in a location much closer to the soil-root plate hinge, forming small mounds of soil and rock where there previously were none, in the fashion of 'soil and rock fulcrum' that forms close to the hinge point. This, although strongly depending on the cohesion level of the soil, would effectively create a physical impediment to the trees returning to their original position.

The introduction of an energy-based approach aims to provide a clearer response about the hysteretic behaviour that emerged from the M-θ curves. Evaluation of the dissipated (and residual) energy in relation to the maximum energy input at that point, namely the ratios $E_{Dis,i}/E_{Max,i}$ and $E_{Res,i}/E_{Max,c,i}$ (Fig. 3 and Fig. 12), provides robust data about the time of the onset of hysteresis in the tree. The first takes the single cycle as an observational unit, whereas the latter analyse the response from a global perspective (i.e., evaluates energy from the initial undisturbed condition up to the i^{th} load cycle). The ratio $E_{Dis,i}/E_{Max,i}$, in the pre-peak phase is on average approximately ≈ 0.15 and never above 0.4. The second ratio $E_{Res,i}/E_{Max,c,i}$, shows that in a few cases within small normalised maximum rotation ($\theta_0 < 0.2$), the residual irreversible rotations can absorb up to 50 % of the input energy. However, comparing the dissipated energy with respect to the one calculated at the peak moment $E_{Dis,i}/E_{Max,Peak}$ (Fig. 13) shows that the largest contributions are the ones toward rotations near collapse conditions. Thus, energy dissipation may be already involved even at small values of base rotation, although the magnitude at near collapse condition can be up to two orders of magnitude higher than the one evaluated over the initial cycles.

Given the uncertainty in defining a clear limit for the elastic response of a tree using traditional approaches, the energy approach employed in this study may support providing a more legitimate definition of the boundaries and properties of the elastic and inelastic responses of trees subject to cycling loads. For example, such a limit may correspond to a threshold of the ratio $E_{Dis,i}/E_{Max,Peak}$, which expresses the energy dissipation of the root-plate system with respect to the maximum input energy that can be absorbed before reaching peak resistance (Fig. 12b). Based on our results, such a value may be set between 0.3 and 0.4 times $\theta(M_{Peak})$ below which the tree dissipates less than 1 % of $E_{Max,Peak}$ in 18 out of 20 load cycles. Transforming it in absolute terms implies that for load cycles with peak rotations $\theta(M_{Max})$ up to 1.6–1.8° (see supplementary material) no valuable energy dissipation and damages are encountered. This threshold would be definitely higher than the actual reference values of rotations that assume an elastic response (Lundström et al., 2007; Marchi et al., 2022; Wessolly and Erb, 1998). This can be seen by plotting the energy content superimposed on the values of base rotations (Fig. 11).

An additional value about the use of energy as descriptor for the resistance of trees is the potential prediction of the total input energy causing the tree failure $E_{Max,Peak}$ as well as the cumulative energy $E_{Max,c}$ at various reference rotations, through common allometric predictors related to the tree size. This was proved also in our study where we found positive correlations with both M_{Peak} and DBH^2xH using available datasets collected with previous test campaigns. This result was independent of the slope of the terrain considered in the analysis, which have been demonstrated to impact the values of the critical wind speeds as shown by Costa et al. (2023).

The concept of maximum energy that can be absorbed by a tree before it reaches mechanical failure can replace a more static approach such as the one currently used for calculating critical wind speed. In this case instead of using a probabilistic approach that correlates the critical wind speed of damage with a measure of wind speed - whether hourly

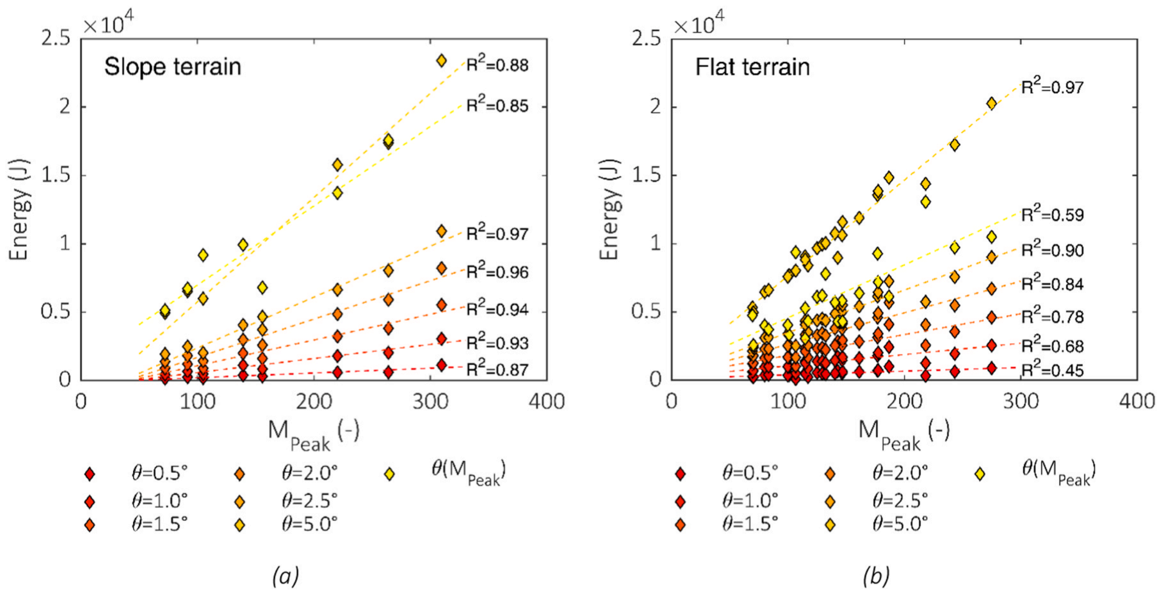

Fig. 14. $E_{Max,c,i}$ at increasing values of base rotation vs. M_{Peak}.

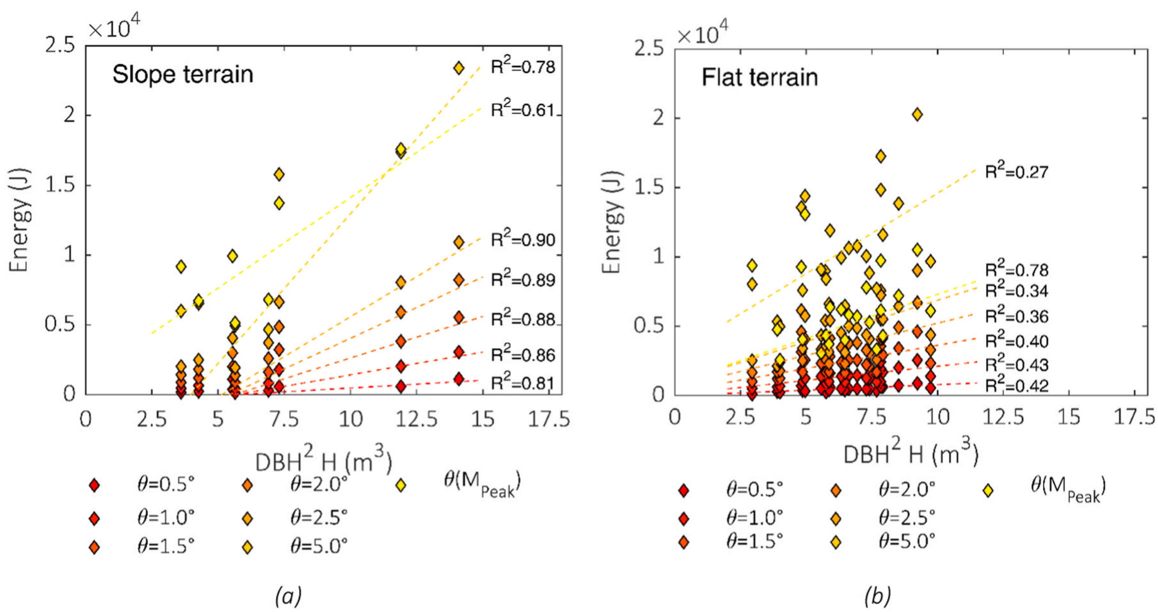

Fig. 15. $E_{Max,c,i}$ at increasing values of base rotation vs. DBH^2xH.

mean, or gust - it appears possible to introduce the concept of damage accumulated by different gusts until a damage point is reached, either for stem breakage or overturning. Once this concept is established and formulated, the dynamic forest landscape models that simulate wind disturbances could also be updated to more accurately simulate the damage expected during a storm. Following this approach, an important issue to be solved is to analyse wind speed time-series and derive strength and likelihood of the number of gusts that may struck the tree (Dupont, 2016; Finnigan and Shaw, 2000).

5. Conclusions

This study investigated the mechanical response of Norway spruce trees to repeated lateral loads by performing consecutive pulling tests. The procedure allowed us to explore both pre-peak and post-peak phases with consecutive load cycles. The loading mimicked medium-term strong winds and, similarly to previous studies, uprooting was the only observed failure mode. Results were analysed via a classical equilibrium approach as well as through an innovative energy-base methodology which fits with cyclic testing procedures.

Within the pre-peak phase, trees in some cases exhibited a fully elastic response followed by an abrupt change in stiffness near the peak resistance, while other trees exhibited a more linear response with progressive damage accumulation after each load cycle.

This research explored pulling beyond the peak resistance, revealing that trees can withstand some additional stress beyond the peak resistance before complete failure. However, long-term stability is compromised. Even after peak loads, the tree may still exhibit elastic behaviour, albeit with compromised and reduced stiffness. Small but measurable residual rotations were measured after each load repetition, indicating permanent damage even in seemingly undamaged trees.

The study introduced an energy-based approach to analyse tree response. This approach showed promise in: (i) identifying the onset of inelastic behaviour; (ii) defining the elastic limit for trees under cyclic loading; (iii) predicting failure based on the energy absorbed by the tree. In conclusion, the study suggests that the energy-based approach can be a valuable tool for understanding the response of trees to wind loading and potentially improve wind damage prediction in models that include dynamic effects and could simulate windflow. However, further research is needed to address issues such as the total number of effective wind gusts expected during a storm.

Funding

This research was founded by the Department of Land, Environment, Agriculture and Forestry, University of Padova (TESAF) under the "young researchers for VAIA" initiative of the PhD LERH Program of the Università degli Studi di Padova and by the VAIA-Front project and within the Agritech National Research Center and received funding from the European Union Next-GenerationEU (PIANO NAZIONALE DI RIPRESA E RESILIENZA (PNRR) – MISSIONE 4 COMPONENTE 2, INVESTIMENTO 1.4 – D.D. 1032 17/06/2022, CN00000022).

CRediT authorship contribution statement

Maximiliano Costa: Writing – review & editing, Resources, Methodology, Investigation. **Tommaso Locatelli:** Writing – review & editing, Supervision. **Luca Marchi:** Writing – original draft, Visualization, Methodology, Formal analysis, Data curation, Conceptualization. **Barry Gardiner:** Writing – review & editing, Supervision. **Emanuele Lingua:** Project administration, Funding acquisition.

Declaration of Competing Interest

The authors declare that they have no known competing financial interests or personal relationships that could have appeared to influence the work reported in this paper.

Data availability

I have shared the link on the raw data in the reference list

Acknowledgements

Grateful thanks go to the staff of VenetoAgricoltura and Centro Forestale Sede di Pian Cansiglio (BL) for their support during experimentation and to TrentinoRope S.r.l. for supplying cables and relative equipment.

Appendix A. Supporting information

Supplementary data associated with this article can be found in the online version at doi:10.1016/j.foreco.2024.122071.

References

Ancelin, P., Courbaud, B., Fourcaud, T., 2004. Development of an individual tree-based mechanical model to predict wind damage within forest stands. Ecol. Manag. 203, 101–121. https://doi.org/10.1016/j.foreco.2004.07.067.

Blackwell, P.G., Rennolls, K., Coutts, M.P., 1990. A root anchorage model for shallowly rooted Sitka spruce. Forestry 63, 73–91. https://doi.org/10.1093/forestry/63.1.73.

Chen, Y.-Y., Gardiner, B., Pasztor, F., Blennow, K., Ryder, J., Valade, A., Naudts, K., Otto, J., McGrath, M.J., Planque, C., Luyssaert, S., 2018. Simulating damage for wind storms in the land surface model ORCHIDEE-CAN (revision 4262). Geosci. Model Dev. 11, 771–791. https://doi.org/10.5194/gmd-11-771-2018.

Costa, M., Gardiner, B., Locatelli, T., Marchi, L., Marchi, N., Lingua, E., 2023. Evaluating wind damage vulnerability in the Alps: a new wind risk model parametrisation. Agric. Meteor. 341, 109660 https://doi.org/10.1016/j.agrformet.2023.109660.

Coutts, M.P., 1986. Components of tree stability in sitka spruce on peaty gley soil. Forestry 59, 173–197. https://doi.org/10.1093/forestry/59.2.173.

Detter, A., Rust, S., Krišāns, O., 2023. Experimental test of non-destructive methods to assess the anchorage of trees. Forests 14, 533. https://doi.org/10.3390/f14030533.

Detter, A., Rust, S., Jannis Böttcher, Bouillon, J., 2019. Ambient influences on the results of non-destructive pulling tests, in: Proceedings of the 21st Non-Destructive Testing and Evaluation of Wood Symposium.

Dorren, L.K.A., Berger, F., 2006. Stem breakage of trees and energy dissipation during rockfall impacts. Tree Physiol. 26, 63–71. https://doi.org/10.1093/treephys/26.1.63.

Dupont, S., 2016. A simple wind–tree interaction model predicting the probability of wind damage at stand level. Agric. Meteor. 224, 49–63. https://doi.org/10.1016/j.agrformet.2016.04.014.

Finnigan, J.J., Shaw, R.H., 2000. A wind-tunnel study of airflow in waving wheat: an EOF analysis of the structure of the large-eddy motion. Bound. Layer. Meteor. 96, 211–255. https://doi.org/10.1023/A:1002618621171.

Gardiner, B., 2021. Wind damage to forests and trees: a review with an emphasis on planted and managed forests. J. For. Res. 26, 248–266. https://doi.org/10.1080/13416979.2021.1940665.

Gardiner, B., Achim, A., Nicoll, B., Ruel, J.-C., 2019. Understanding the interactions between wind and trees: an introduction to the IUFRO 8th Wind and Trees Conference (2017). For.: Int. J. For. Res. 92, 375–380. https://doi.org/10.1093/forestry/cpz044.

Gardiner, B., Berry, P., Moulia, B., 2016. Review: Wind impacts on plant growth, mechanics and damage. Plant Sci. 245, 94–118. https://doi.org/10.1016/j.plantsci.2016.01.006.

Gardiner, B., Byrne, K., Hale, S., Kamimura, K., Mitchell, S.J., Peltola, H., Ruel, J.-C., 2008. A review of mechanistic modelling of wind damage risk to forests. Forestry 81, 447–463. https://doi.org/10.1093/forestry/cpn022.

Gardiner, B., Peltola, H., Kellomäki, S., 2000. Comparison of two models for predicting the critical wind speeds required to damage coniferous trees. Ecol. Model. 129, 1–23. https://doi.org/10.1016/S0304-3800(00)00220-9.

Gliksman, D., Averbeck, P., Becker, N., Gardiner, B., Goldberg, V., Grieger, J., Handorf, D., Haustein, K., Karwat, A., Knutzen, F., Lentink, H.S., Lorenz, R., Niermann, D., Pinto, J.G., Queck, R., Ziemann, A., Franzke, C.L.E., 2023. Review article: A European perspective on wind and storm damage – from the meteorological background to index-based approaches to assess impacts. Nat. Hazards Earth Syst. Sci. 23, 2171–2201. https://doi.org/10.5194/nhess-23-2171-2023.

Jackson, T.D., Sethi, S., Dellwik, E., Angelou, N., Bunce, A., van Emmerik, T., Duperat, M., Ruel, J.-C., Wellpott, A., Van Bloem, S., Achim, A., Kane, B., Ciruzzi, D. M., Loheide II, S.P., James, K., Burcham, D., Moore, J., Schindler, D., Kolbe, S., Wiegmann, K., Rudnicki, M., Lieffers, V.J., Selker, J., Gougherty, A.V., Newson, T., Koeser, A., Miesbauer, J., Samelson, R., Wagner, J., Ambrose, A.R., Detter, A., Rust, S., Coomes, D., Gardiner, B., 2021. The motion of trees in the wind: a data synthesis. Biogeosciences 18, 4059–4072. https://doi.org/10.5194/bg-18-4059-2021.

James, K., Hallam, C., Spencer, C., 2013. Measuring tilt of tree structural root zones under static and wind loading. Agric. Meteor. 168, 160–167. https://doi.org/10.1016/j.agrformet.2012.09.009.

Jonsson, M.J., Foetzki, A., Kalberer, M., Lundström, T., Ammann, W., Stöckli, V., 2006. Root-soil rotation stiffness of Norway spruce (Picea abies (L.) Karst) growing on subalpine forested slopes. Plant Soil 285, 267–277. https://doi.org/10.1007/s11104-006-9013-7.

Kamimura, K., Nanko, K., Matsumoto, A., Ueno, S., Gardiner, J., Gardiner, B., 2022. Tree dynamic response and survival in a category-5 tropical cyclone: The case of super typhoon Trami. Sci. Adv. 8, 7891. https://doi.org/10.1126/sciadv.abm7891.

Klein, R., Koeser, A., Hauer, R., Hansen, G., Escobedo, F., 2019. Risk assessment and risk perception of trees: a review of literature relating to arboriculture and urban forestry. Arboric. Urban 45. https://doi.org/10.48044/jauf.2019.003.

Laurance, W.F., Curran, T.J., 2008. Impacts of wind disturbance on fragmented tropical forests: a review and synthesis. Austral Ecol. 33, 399–408. https://doi.org/10.1111/j.1442-9993.2008.01895.x.

Leigh, W., 2014. Low cycle fatigue failure of a sitka spruce tree in hurricane winds. Arboric. Urban 40, 272–285. https://doi.org/10.48044/jauf.2014.026.

Linhares, C.S.F., Gonçalves, R., Martins, L.M., Knapic, S., 2021. Structural stability of urban trees using visual and instrumental techniques: a review. Forests 12, 1752. https://doi.org/10.3390/f12121752.

Lundstrom, T., Jonas, T., Stockli, V., Ammann, W., 2007. Anchorage of mature conifers: resistive turning moment, root-soil plate geometry and root growth orientation. Tree Physiol. 27, 1217–1227. https://doi.org/10.1093/treephys/27.9.1217.

Lundstrom, T., Jonsson, M.J., Volkwein, A., Stoffel, M., 2009. Reactions and energy absorption of trees subject to rockfall: a detailed assessment using a new experimental method. Tree Physiol. 29, 345–359. https://doi.org/10.1093/treephys/tpn030.

Lundström, T., Jonsson, M.J., Kalberer, M., 2007. The root–soil system of Norway spruce subjected to turning moment: resistance as a function of rotation. Plant Soil 300, 35–49. https://doi.org/10.1007/s11104-007-9386-2.

Marchi, L., 2019. Safety assessment of trees used as anchors in cable-supported tree harvesting based on experimental observations. Biosyst Eng. https://doi.org/10.1016/j.cis.2019.03.005.

Marchi, L., Costa, M., Grigolato, S., Lingua, E., 2022. Overturning resistance of large diameter Norway spruce (Picea abies (L.) Karst) on sloped conditions. Ecol. Manag. 524, 120531 https://doi.org/10.1016/j.foreco.2022.120531.

Marchi, L., Grigolato, S., Lingua, E., Cavalli, R., 2023. Tree_pulling_Data_Norway Spruce_Italian Alps [WWW Doc.]. https://doi.org/10.25430/researchdata.cab.unipd.it.00000387.

Marchi, L., Mologni, O., Grigolato, S., Cavalli, R., 2020. Evaluation on the stability of tree used as anchors in cable yarding operations: a preliminary test based on low-cost MEMS sensors. : Lect. Notes Civ. Eng. 473–479. https://doi.org/10.1007/978-3-030-39299-4_53.

Marchi, L., Mologni, O., Trutalli, D., Scotta, R., Cavalli, R., Montecchio, L., Grigolato, S., 2019. Safety assessment of trees used as anchors in cable-supported tree harvesting based on experimental observations. Biosyst. Eng. 186, 71–82. https://doi.org/10.1016/j.biosystemseng.2019.06.022.

Marchi, L., Trutalli, D., Mologni, O., Gallo, R., Roeser, D., Cavalli, R., Grigolato, S., 2021. Mechanical response of natural anchors in cable logging. Int. J. For. Eng. 32, 29–42. https://doi.org/10.1080/14942119.2021.1826882.

Moore, J.R., 2000. Differences in maximum resistive bending moments of Pinus radiata trees grown on a range of soil types. Ecol. Manag. 135, 63–71. https://doi.org/10.1016/S0378-1127(00)00298-X.

Moore, J.R., Maguire, D.A., 2004. Natural sway frequencies and damping ratios of trees: concepts, review and synthesis of previous studies. Trees - Structure and Function 18, 195–203. https://doi.org/10.1007/s00468-003-0295-6.

Neild, S.A., Wood, C.J., 1999. Estimating stem and root-anchorage flexibility in trees. Tree Physiol. 19, 141–151. https://doi.org/10.1093/treephys/19.3.141.

Nicoll, B.C., Gardiner, B.A., Rayner, B., Peace, A.J., 2006. Anchorage of coniferous trees in relation to species, soil type, and rooting depth. Can. J. For. Res. 36, 1871–1883. https://doi.org/10.1139/x06-072.

Nielsen, C.N., 2011. Træers forankring er meget mere dynamisk og omskiftelig end hidtil antaget. Skoven 3, 137–139.

Nykänen, M.-L., Peltola, M., Quine, C., Kellomäki, S., Broadgate, M., 1997. Factors affecting snow damage of trees with particular reference to european conditions. Silva Fenn. 31, 193–213.

O'Sullivan, M.F., Ritchie, R.M., 1993. Tree stability in relation to cyclic loading. Forestry 66, 69–82. https://doi.org/10.1093/forestry/66.1.69.

Patacca, M., Lindner, M., Lucas-Borja, M.E., Cordonnier, T., Fidej, G., Gardiner, B., Hauf, Y., Jasinevičius, G., Labonne, S., Linkevičius, E., Mahnken, M., Milanovic, S., Nabuurs, G., Nagel, T.A., Nikinmaa, L., Panyatov, M., Bercak, R., Seidl, R., Ostrogović Sever, M.Z., Socha, J., Thom, D., Vuletic, D., Zudin, S., Schelhaas, M., 2023. Significant increase in natural disturbance impacts on European forests since 1950. Glob. Chang Biol. 29, 1359–1376. https://doi.org/10.1111/gcb.16531.

Peltola, H., Kellomäki, S., Hassinen, A., Granander, M., 2000. Mechanical stability of Scots pine, Norway spruce and birch: an analysis of tree-pulling experiments in Finland. Ecol. Manag. 135, 143–153. https://doi.org/10.1016/S0378-1127(00)00306-6.

Peltola, H., Kellomäki, S., Väisänen, H., Ikonen, V.-P., 1999. A mechanistic model for assessing the risk of wind and snow damage to single trees and stands of Scots pine, Norway spruce, and birch. Can. J. For. Res. 29, 647–661. https://doi.org/10.1139/cjfr-29-6-647.

Quine, C.P., Gardiner, B.A., Moore, J., 2021. Wind disturbance in forests: The process of wind created gaps, tree overturning, and stem breakage. In: Plant Disturbance Ecology. Elsevier, pp. 117–184. https://doi.org/10.1016/B978-0-12-818813-2.00004-6.

Raupach, M.R., 1992. Drag and drag partition on rough surfaces. Bound. Layer. Meteor. 60, 375–395. https://doi.org/10.1007/BF00155203.

Raupach, M.R., 1994. Simplified expressions for vegetation roughness length and zero-plane displacement as functions of canopy height and area index. Bound. Layer. Meteor. 71, 211–216. https://doi.org/10.1007/BF00709229.

Raupach, M.R., 1995. Corrigenda. Bound. Layer. Meteor. 76, 303–304. https://doi.org/10.1007/BF00709356.

Rodgers, M., Casey, A., McMenamin, C., Hendrick, E., 1995. An experimental investigation of the effects of dynamic loading on coniferous trees planted on wet mineral soils. In: Coutts, M.P., Grace, J. (Eds.), Wind and Trees. Cambridge University Press, Cambridge, pp. 204–219.

Romagnoli, F., Cadei, A., Costa, M., Marangon, D., Pellegrini, G., Nardi, D., Masiero, M., Secco, L., Grigolato, S., Lingua, E., Picco, L., Pirotti, F., Battisti, A., Locatelli, T., Blennow, K., Gardiner, B., Cavalli, R., 2023. Windstorm impacts on European forest-related systems: An interdisciplinary perspective. https://doi.org/10.1016/j.foreco.2023.121048.

Schindler, D., Kolbe, S., 2020. Assessment of the response of a Scots pine tree to effective wind loading. Forests 11, 145. https://doi.org/10.3390/f11020145.

Schindler, D., Mohr, M., 2018. Non-oscillatory response to wind loading dominates movement of Scots pine trees. Agric. Meteor. 250–251, 209–216. https://doi.org/10.1016/j.agrformet.2017.12.258.

Schindler, D., Mohr, M., 2019. No resonant response of Scots pine trees to wind excitation. Agric. Meteor. 265, 227–244. https://doi.org/10.1016/j.agrformet.2018.11.021.

Seidl, R., Rammer, W., Spies, T.A., 2014. Disturbance legacies increase the resilience of forest ecosystem structure, composition, and functioning. Ecol. Appl. 24, 2063–2077. https://doi.org/10.1890/14-0255.1.

Silins, U., Lieffers, V.J., Bach, L., 2000. The effect of temperature on mechanical properties of standing lodgepole pine trees. Trees 14, 424–428. https://doi.org/10.1007/s004680000065.

Spatz, H.C., Theckes, B., 2013. Oscillation damping in trees. Plant Science 207, 66–71. https://doi.org/10.1016/J.PLANTSCI.2013.02.015.

Stokes, A., Salin, F., Kokutse, A.D., Berthier, S., Jeannin, H., Mochan, S., Dorren, L., Kokutse, N., Abd.Ghani, M., Fourcaud, T., 2005. Mechanical resistance of different tree species to Rockfall in the French Alps. Plant Soil 278, 107–117. https://doi.org/10.1007/s11104-005-3899-3.

The MathWorks Inc., 2023. MATLAB 2023a.

Václav, S., Jan, T., Vinko, P., Luděk, P., Barbora, V., Martin, B., Jaromír, M., 2021. Influence of soil in oak root system on its response to bending, in: 9th Hardwood Conference, An Underutilized Resource: Hardwood Oriented Research. pp. 83–89..

Wessolly, L., 1996. Standsicherheit von Bäumen. Der Kippvorgang ist geklärt. Stadt. und Gr. üN. 4, 268–272.

Wessolly, L., Erb, M., 1998. Handbuch der Baumstatik und Baumkontrolle [Manual of Tree Statics and Tree Inspection]. Patzer Verlag, Berlin, Germany.